NANO LETTERS

Letter

pubs.acs.org/NanoLett

Directed Self-Assembly of Micron-Sized Gold Nanoplatelets into Oriented Flexible Stacks with Tunable Interplate Distance

Hanumantha Rao Vutukuri,*[,§] Stéphane Badaire,[§] D. A. Matthijs de Winter,[+] Arnout Imhof,[§] and Alfons van Blaaderen*[,§]

[§]Soft Condensed Matter, Debye Institute for Nanomaterials Science, Utrecht University, Princetonplein 1, 3584 CC, Utrecht, The Netherlands

[+]Department of Biology, Utrecht University, Padualaan 8, 3584 CH, Utrecht, The Netherlands

Supporting Information

ABSTRACT: A growing demand for control over the interparticle spacing and the orientation of anisotropic metallic particles into self-assembled structures is fuelled by their use in potential applications such as in plasmonics, catalysis, sensing, and optoelectronics. Here, we present an improved high yield synthesis method to fabricate micron- and submicron-sized gold nanoplatelets with a thickness less than 20 nm using silver nanoplatelets as seeds. By tuning the depth of the secondary minimum in the DLVO interaction potential between these particles, we are able to assemble the platelets into dynamic and flexible stacks containing thousands of platelets arranged face-to-face with well-defined spacing. Moreover, we demonstrate that the length of the stacks, and the interplate distance can be controlled between tens and hundreds of nm with the ionic strength. We use a high frequency external electric field to control the orientation of the stacks and direct the stacks into highly organized 2D and 3D assemblies that strongly polarize light.

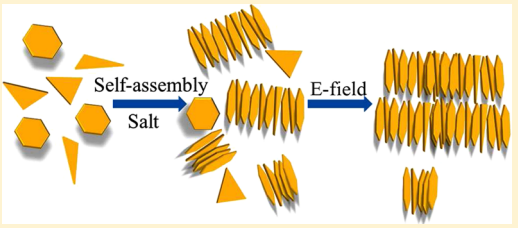

KEYWORDS: *Gold nanoplatelets, directed self-assembly, DLVO potential, flexible stacks, electric fields, plasmonics*

Over the last few decades, a wide variety of nanoparticle systems with well-defined shapes have become available.[1−3] The quest to control the self-assembly of such nanoparticles into ordered superlattices, especially if one of the components is a metallic nanoparticle,[4−8] is fuelled by a demand for new types of materials, where new collective properties such as a negative refractive index[9−11] can emerge from the individual building blocks as well as from the coupling between the building blocks. Several methods have been reported to fabricate nanocrystal superstructures, including: evaporation of solvent at an air−liquid interface,[12,13] phase separation induced by attractions through a depletion interaction,[14,15] by the addition of an antisolvent,[16,17] and more specific interactions which can be induced by DNA molecules[18−22] and external fields.[6,23−26]

Surface plasmons of metallic nanoparticles are collective surface modes of the conduction electrons that can be excited by electromagnetic radiation, which can lead to very large locally enhanced electric fields. Because of these locally enhanced electric fields, surface plasmons are useful in many applications such as metamaterials with a negative refractive index,[9−11] surface enhanced Raman scattering,[7,27−32] photovoltaics,[4,5] catalysis,[33−35] and (opto)electronics.[31] If the metallic nanoparticles are arranged in one, two, or three-dimensional (1D−3D) assemblies with distances between the particles that are small enough, the plasmonic modes can couple and additional degrees of freedom to tune their properties become available.[11] Additionally, for anisotropic particles, the symmetry as compared to spherical particles is reduced and results in plasmonic modes reflecting the different symmetries and aspect ratio(s).[2,7,8]

In this paper we focus on micron-sized plate-like gold (Au) nanoparticles where the shape anisotropy, characterized by the ratio (a/b) of the plate diameter a and plate thickness b, is as large as 50. However, the number of studies on noble metal particles with a plate-like morphology is significantly less than other anisotropic shapes, probably because of the lack of convenient synthetic procedures to produce such particles in high yield.[15,28,36] As far as we know, even recently improved methods still produce a significant percentage of differently shaped Au particles, like rods and/or spheres, as well.[37,38] With these methods, a high purity of plates can only be achieved through separation methods such as repeated centrifugation or methods that involve inducing shape specific attractions using a depletion agent[15] or DNA supramolecular chemistry.[21] Self-assembled structures of plate-like noble metal particles, such as 1D stacks of platelets, are even rare, and we are aware of only a few examples.[15,28,36] Here we show how the yield of an existing method developed by Hachisu et al. to synthesize gold nanoplates[36] can be significantly improved by using Ag nanoplates as seeds. We self-assemble these gold plates into

Received: June 16, 2015
Revised: July 20, 2015
Published: August 3, 2015

DOI: 10.1021/acs.nanolett.5b02384
Nano Lett. 2015, 15, 5617−5623

flexible 1D stacks that contain thousands of plates with well-defined spacing between them without using surfactants that act as depletion inducing agents[15] or spacer molecules attached to the metal surface.[28] We further show an exquisite control over the interplate spacing from tens to hundreds of nm simply by changing the ionic strength of the solution. Moreover, we use external electric fields to align and direct the self-assembly (SA) of these stacks, providing control over the anisotropy of the structures over millimeter-sized regions.

Synthesis and Characterization of Au Nanoplatelets. It is possible to generate Au nanoplatelets by top-down methods like lithography. However, we focus here on wet chemical methods which allows for the production of sufficient quantity of particles necessary for SA experiments. Several methods to produce Au nanoplatelets are available that differ in the stabilizer that is used to stabilize the resulting particles and/or differ in the reducing agent of the gold cations. These methods make use of the surfactant cetyltrimethylammonium bromide (CTAB) as the stabilizer;[27,37] the polymer polyvinylpyrolidone (PVP) as the protecting agent, and ethylene glycol (EG) as the reducing agent as in the "polyol" process;[39,40] photochemically induced reduction processes;[41,42] biomolecules inspired reducing agents or stabilizers;[43−45] salicylic acid as both the stabilizer and reducing agent;[8,36] and oxidative etching.[46] For a more complete list of methods, see e.g., the review papers 2 and 8. We note that, while the production yield of synthesis methods has improved, these methods[37,38] still produce significant amounts of other particle shapes as well.[37,38] To circumvent this, we chose to adapt the method of Hachisu et al.[36] as it combines the role of stabilizer and reducing agent in one molecule, salicylic acid, and the method is thus surfactant free. We found (for details see the Materials and Methods section) that by using small sub 100 nm sized silver nanoprisms[47] (see Figure S1) as seeds the yield of Au nanoplatelets could be increased significantly to about 75−80% based on the number of platelets (with the remaining percentage of particles composed of ∼100 nm sized spherical particles that are easily removed by a single centrifugation step). Figure 1a shows the scanning electron microscopy (SEM) image of Au nanoplatelets in a typical synthesis. Transmission electron microscopy (TEM) image, and the corresponding selected-area electron diffraction (SAED) patterns were used to characterize the crystallinity (Figure 1c) of the particles. The SAED pattern clearly reveals that the Au nanoplatelet is single crystalline. We believe that the contrast within the triangle particle is the result of the internal stress, which comes from the bending of the thin sheet.[39,41,43] The two-dimensional energy dispersive X-ray spectroscopy (EDX) maps reveal that the Ag seeds were not present anymore in the final product (see Figure S2). We believe that the Ag seeds have dissolved and were replaced with Au during the growth process as has been reported for other particles systems.[48] It is important to mention here that although the focus of the present paper was on the use and self-assembly of micron-sized nanoplatelets because of their easier visualization with light microscopy on the single particle level, significantly smaller platelets that also can form stacks are available through the same synthesis protocol by adjusting the concentration of chloroauric acid (results not shown). The gold nanoplates used in the present experiments, consisted of triangular and hexagonal particles (see Figure 1a). The average edge length of the obtained triangular particles was 670 ± 65 nm and hexagonal particles were 525 ± 45 nm. The thickness of both particles was about

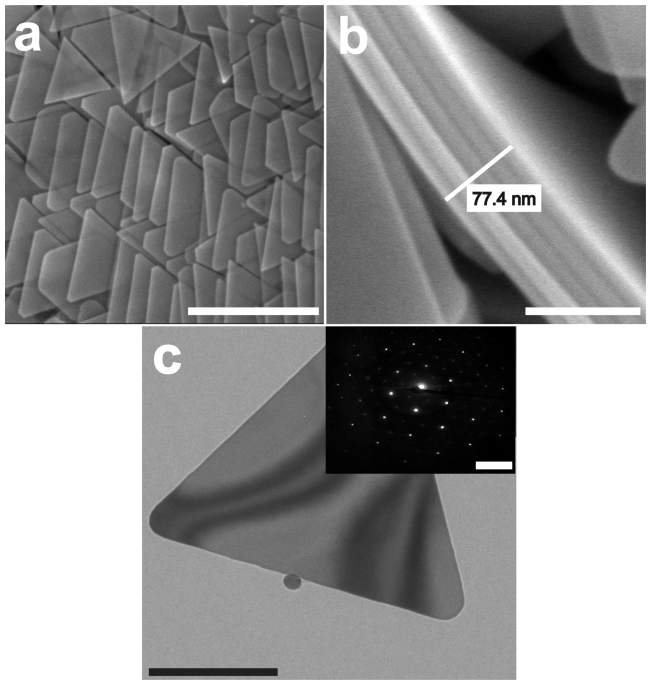

Figure 1. Scanning electron micrographs of thin gold platelets. (a) Triangular (and cut-triangular) and hexagonal-shaped gold platelets. (b) The total thickness of a stack of 5 platelets shows that the average thickness of gold platelet is about 16 nm. (c) A high angle annular dark field scanning transmission electron microscopy image of gold nanoplatelet. The inset shows the selected-area electron diffraction (SAED) pattern. Scale bars are 1.0 μm (a), 100 nm (b), 300 nm (c); the inset scale bar is 100 nm^{-1}.

16 nm (see Figure 1b). It is interesting to mention that recently a procedure has been developed in which the polygonal shapes of gold nanoplatelets can be turned into a well-defined disk shape by a preferential etching procedure.[49] This procedure could thus significantly increase the monodispersity in shape,[49] if necessary, but was not used in the present study. The surface potential of the resulting Au plates was determined by electrophoresis to be −35 mV in water and −40 mV in 30 wt % glycerol solution that was also used in some of the SA experiments.

Self-Assembly of Au Nanoplatelets without Electric Field. We first studied the phase behavior of the gold platelets at various salt concentrations. In the absence of salt, the particles remained stable and isotropically dispersed as shown in Figure 2a. Due to the high density of gold (19.3 g/cm^3) and the volume of the Au platelets, the particles sedimented within minutes to the bottom of the sample cell, increasing the local volume fraction significantly. We did not observe any order formation such as a liquid crystal phase. Apparently, the effective aspect ratio of the particles was reduced enough at this ionic strength, and/or the osmotic pressure exerted by gravity was not sufficient, to induce a phase transition.

At low salt concentrations (<0.5 mM), the particles still remained stable and well-dispersed. We did not see any order formation over time. On the other hand, after 5 min, at 0.5 mM particles started self-assembling into small flexible 1D stacks (<5 μm) in which the platelets arranged in face-to-face fashion, in coexistence with individual particles. We did not observe any further growth of columns with time, apparently the system had reached a steady state. As the salt concentration was further increased to 0.8 mM, we first observed stacks of about 5−15

DOI: 10.1021/acs.nanolett.5b02384
Nano Lett. 2015, 15, 5617−5623

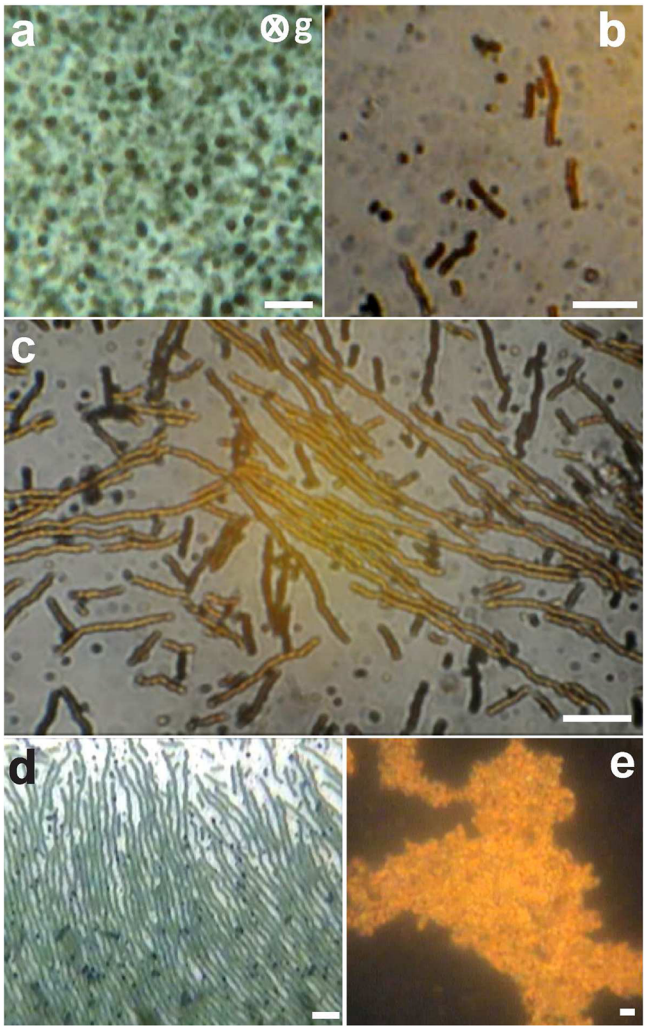

Figure 2. Optical micrographs showing the phase behavior of the gold platelets for various salt concentrations. (a) The particles isotropically dispersed in water at zero salt concentration, (b) after 5 min of waiting time at 0.8 mM of KCl, (c) after 60−70 min of waiting time at 0.8 mM of KCl, and (d) after 3 h of waiting time at 1.5 mM of KCl. (e) At higher salt concentrations ≥2.0 mM of KCl, particles aggregated irregularly and irreversibly. The direction of gravity is perpendicular to the plane in each image. Scale bars are 15 μm.

μm in length (Figure 2b). After 60−70 min, these stacks had grown further into longer columns (~150 μm), resulting in stacks containing several thousands of plates (Figure 2c). When we increased both the salt concentration (1.5 mM) and waiting time (60−70 min), most of the particles assembled into very long columns (>500 μm). After 3 h, we observed a local nematic order of these longer stacks (Figure 2d).

We note that the particles forming the columns were individually in Brownian motion, and also the columns themselves showed active Brownian motion (see Movie S1), which became slower when the stack sizes increased. Moreover, theses columns appeared to be dynamic in the sense that longer columns were seen to split up or grow by joining of new single particles or by merging with short columns, again, ultimately forming a steady state. When the salt concentration was within the range from 0.8 to 2.0 mM, both ends of the columns were continuously seen to capture particles or short columns moving around within close proximity, thus growing into longer columns as shown in Figure 2c and d. At higher salt concentrations (≥2.0 mM), the platelets immediately (<1 min) started aggregating irregularly (Figure 2e), and we did not observe the Brownian motion of individual particles.

In order to understand the observed self-assembly behavior (Figure 2), we calculated the interaction potential between two gold platelets facing each other as a function of the interplatelet distance for different salt concentrations as shown in Figure 3.

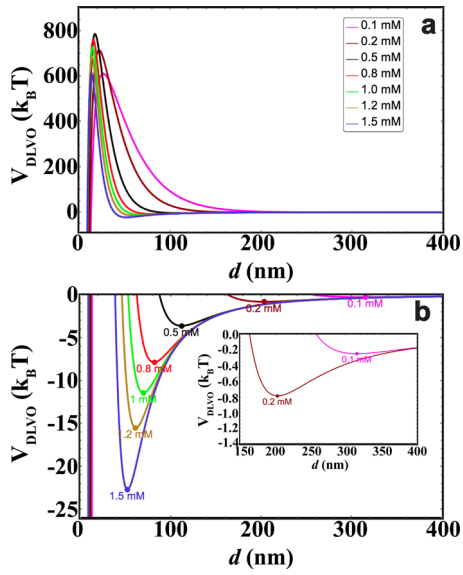

Figure 3. DLVO potential between two gold platelets of size 0.17 μm^2, surface potential −35 mV in water. Interaction potentials were calculated as a function of the interplatelet distance d for different 1−1 salt concentrations. (a) DLVO potential. (b) The secondary minimum of the DLVO potential.

Moreover, we included retardation effects in our DLVO (Derjaguin, Landau, Vervey, and Overbeek) potential calculations (see Supporting Information for details). At salt concentrations below 0.1 mM, the double layer repulsion overwhelms the van der Waals attraction at all separations. As a result, the particles remain stable and isotropically dispersed as observed in Figure 2a. Our DLVO calculations clearly demonstrate that the potential energy has a secondary minimum of at least 1 k_BT at an interparticle distance between 50 to 300 nm, for salt concentrations above ≥0.2 mM. At low salt concentrations (0.2−0.4 mM) the depth of the minimum is small, and comparable to the thermal energy (see the inset in Figure 3b). We believe that the strength of the attraction is not strong enough to overcome thermal energy and to form stacks. We note that our calculations are indeed consistent with our experimental observations. On the other hand, the secondary minimum attains a depth of ~ −4 k_BT at 0.5 mM salt concentration when the first signs of stacking were observed. At a higher salt concentration of 0.8 mM, the attractive potential has further deepened to −7 k_BT at an interparticle distance around 90 nm, and one should expect the Au nanoplatelets to start self-assembling into flexible 1D stacks in which the platelets face each other at the distance of the secondary minimum. This behavior was indeed exactly what was observed as shown in Figure 2b, eventually resulting in stacks containing several thousands of platelets (Figure 2c). We note that the similar stack formation of gold plates was observed by Hachisu et al.[36] and attributed to the secondary minimum in the DLVO interaction potential.

DOI: 10.1021/acs.nanolett.5b02384
Nano Lett. 2015, 15, 5617−5623

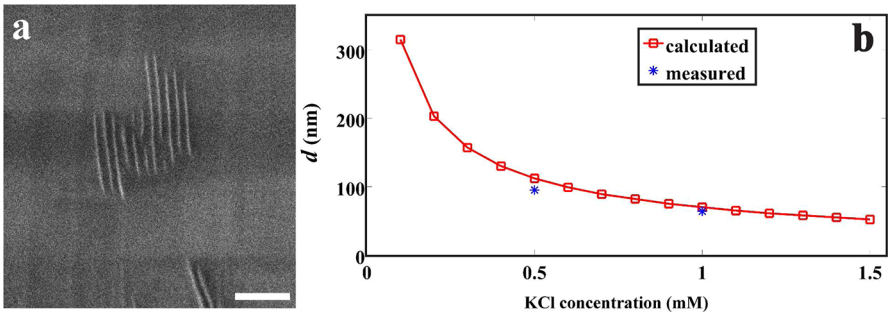

Figure 4. (a) Cryo-scanning electron micrograph. A well-frozen sample was sectioned with a focused ion beam, and subsequently it was imaged with a cryo-SEM. A cross-sectional view of a stack of gold plates shows that the interplatelet distance within a column is uniform and is about 64 nm in a suspension containing 1 mM KCl. (b) The interplatelet spacing (d) for various KCl concentrations. The graph showing the measured (blue circles) and calculated (red squares) distances between the plates for various salt concentrations. The scale bar is 500 nm.

Next, we discuss the effect of gravity on the observed phase behavior. For the particles shown in Figure 2, it can be calculated that the height over which such a nanoplatelet has to be displaced in water to gain k_BT in gravitational energy is about 1.72 μm. This means that a platelet that stands perpendicular to the bottom container wall has a gravitational energy about 1/2 k_BT higher than when it lies flat down onto it (Figure S3). However, the potential difference between a horizontally oriented, isolated particle and a particle trapped in the secondary minimum with another particle is many times higher. Therefore, a particle joining the column gains a significantly larger amount of free energy than an isolated particle on the bottom of the cell.

The interparticle spacing in stacks of gold platelets can play an important role in applications where the collective properties emerging from the individual particles as well as neighboring particles are of importance.[7,11] We demonstrate that the interparticle spacing can be varied by means of the salt concentration. Although the diameter of the plates studied in this paper was of micron length, it is still difficult to measure the interplatelet distance in a column by presently available optical microscopy techniques because of: (i) the small separation of the particles (>60 nm), (ii) active Brownian motion of the columns, and (iii) strong absorption and scattering of light by the individual platelets as well as the stacks. To overcome these limitations, we used cryo-electron microscopy. With this technique the solvent is vitrified fast enough on the diffusion time scale of the particles that the structures are essentially a snapshot in time. The vitrified samples were gradually sectioned with a focused ion beam (FIB) and subsequently imaged by scanning electron microscopy (SEM), under cryo conditions (Figure 4a). To prevent the crystallization of water, which for pure water can be a limitation of this technique, we performed our FIB measurements of nanoplateles SA in a mixture of 30 wt % glycerol in water. In the solvent mixture, the surface potential and SA behavior were similar as in water. (As can be seen in Figure S4, also the interaction energies calculated for this mixture and somewhat larger surface potential of −40 mV were comparable to the curves calculated for the SA in pure water). Figure 4a shows that the interplate distance (d) was about 64 nm in a 1.0 mM suspension. Using the same technique, we measured the interparticle distance for 0.5 mM salt concentration to be 95 nm. Moreover, our experimental measurements are in good quantitative agreement with our DLVO calculations for salt concentrations of 1 mM, whereas the measured value deviated slightly from the DLVO calculations for the 0.5 mM solution (Figure 4b). This discrepancy can be attributed to the fact that the secondary minimum is only about $-4k_BT$, which is not very strong with respect to thermal energy. Young et al.,[15] who created small stacks of Au nanoplates using depletion interactions induced by the surfactant stabilizing their Au platelets, reported much smaller interparticle distances as the surfactant used cetyltrimethylammonium bromide (CTAB) not only acted as depletant, but also increased the ionic strength.

Self-Assembly in an Electric Field. External electric fields have proven to be a robust tool to direct colloidal self-assembly of strings (1D),[50−56] sheets (2D),[57] and equilibrium 3D crystallites.[52,58] Here, a high-frequency field was used to prevent the polarization of the electric double layer around the particle. For a thin gold platelet, the polarizability is different between the major and the minor axis of the particle. The energetically most favorable state is that the particles align with their major axis along the applied field direction. At low field strengths (E_{rms} = 0.025 V μm^{-1}, f = 200 kHz, where E_{rms} is the root-mean-square electric field strength, and f is the frequency) and without added salt, the induced dipole moment in each particle led the platelets to assemble into one particle thick strings that were aligned with their major axis oriented in the field direction as seen in Figure 5a. In the absence of salt, the response of our thin gold platelets is thus similar to that of rods.[23,24] We note that the time scale for chain formation was on the order of a few seconds. However, alignment induced by the electric fields is reversible if the particles are not pushed into distances where the primary van der Waals minimum takes over, so that the stacks lost their orientational ordering whenever the field was switched off.

Next, we investigated the response of gold platelets for two different salt concentrations (0.8 mM and 1.5 mM) in external electric fields. As mentioned, after a short waiting time (~5 min) particles arranged into short (~10−15 μm) flexible stacks (Figure 2b) at a salt concentration of 0.8 mM. When such dispersion was exposed to an external electric field (E_{rms} = 0.015 V μm^{-1}, f = 200 kHz), the columns started to align perpendicular to the applied field direction. However, the major axis of the individual particles within a column was still oriented in the field direction. Figure 5b shows large columns of particles that formed within seconds after applying relatively small field strengths (E_{rms} = 0.015 V μm^{-1}, f = 200 kHz). These structures were more dynamic in terms of growing in length than the columns in the absence of the field. This is indicated by new small columns continuously coming to join both ends, thereby growing into longer columns. Moreover, induced dipolar

DOI: 10.1021/acs.nanolett.5b02384
Nano Lett. 2015, 15, 5617−5623

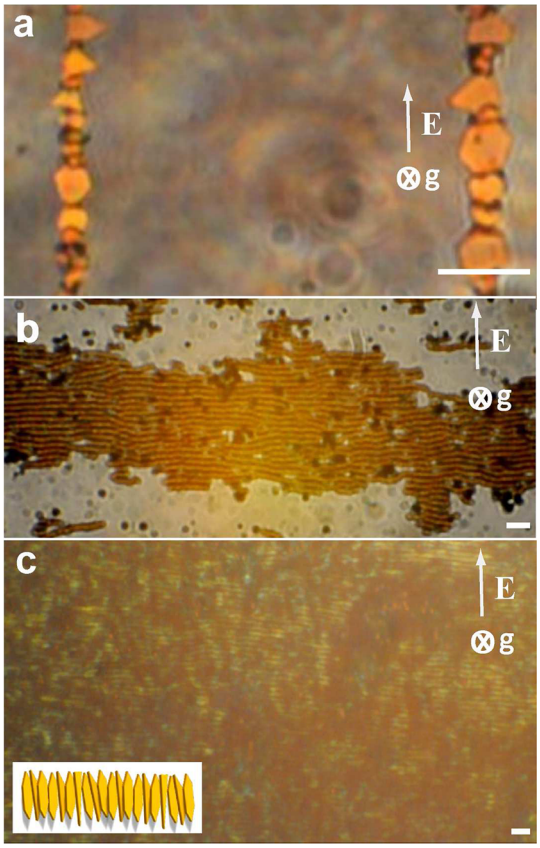

Figure 5. Gold platelets in an external electric field (E_{rms} = 0.015 V μm^{-1}, f = 200 kHz). (a) Optical micrograph of strings of gold platelets in water. The particles became aligned with their longest axis along the field direction. (b–c) Optical micrographs of the directed columnar phase at different salt concentrations in an AC field. (b) A defect-rich columnar phase was observed at 0.8 mM of KCl. (c) A defect-free 2D columnar phase was observed at 1.5 mM of KCl. The lower inset schematically illustrates the orientation of particles in the columns. The directions of the applied electric field and gravity are indicated in each image. Scale bars are 1.0 μm (a), and 5.0 μm (b–c).

attractions between columns forced them to arrange side-by-side because the major axis of the individual particles in a column was in the field direction. Unfortunately, we were not able to see the alignment of particles between the columns on a single particle level, and further theoretical and/or simulations work has to resolve what the exact relationship between the platelets in between columns was. At the salt concentration of 1.5 mM, most of the dispersion transformed into long columns (~ mm) after waiting time of about 1–1.5 h time, (Figure 2c). Even at low field strengths (E_{rms} = 0.01 V μm^{-1}, f = 200 kHz), all of these columns became aligned perpendicular to the field direction and then transformed into a defect-rich 2D columnar phase. After a few minutes, all of the defects annealed out by further merging of the columns. These columns then transformed into a larger 2D columnar phase as shown in Figure 5c. It can also be seen that some columns also started to form on top of the 2D phase (darker patches). When the field strength was further increased (E_{rms} = 0.04 V μm^{-1}, f = 200 kHz), the stacks that were initially aligned perpendicular to the field direction started to rotate slowly, as a result, band formation at nearly 45° relative to the applied field direction, as shown in Figure S5 was observed. The speed and direction of the rotation of platelets within each band depended on the relative position of the columns with respect to the external electric field (see Supporting Information). We believe that these patterns have an electro-hydrodynamic origin and have been observed before for other particle shapes and systems.[59−62] When the field strength was further increased to 0.07 V μm^{-1}, all of the stacks were destroyed within a few seconds due to much stronger electrohydrodynamic flows. Many shorter columns and individual plates formed, which resulted from breakage of longer ones due to a strong rotational motion. When the field was turned off, the particles instantaneously reformed stacks, and these stacks were directed to ordered structures using low field strengths, E_{rms} = 0.015 V μm^{-1}, f = 200 kHz (see Movie S2).

As a first indication of the intriguing optical properties of the SA structures, we proceeded to measure the polarizing effects of the stacks using polarization microscopy on the self-assembly in an external electric field, as shown in Figures 5c and 6. We note

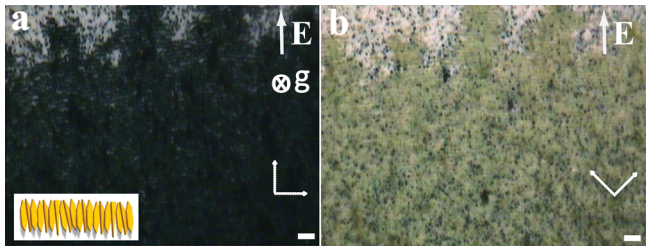

Figure 6. Polarization light micrographs of columns of 1.5 mM dispersion in an electric field. The orientation of the polarizers and the applied electric field are indicated by arrows in the lower-right corner and upper-right corner, respectively. We note that we deliberately rotated one of the polarizers a few degrees off from a perfect 90° in order to distinguish the well-oriented columns of stacks from the background. As a result, the background is not completely black. (a) The orientation of the director parallel to one of the polarizers. (b) The polarizers were orientated at about 45° to the applied field direction. Scale bars are 15 μm.

that when light passes through an ordered phase between crossed polarizers, the orientation of the director is not parallel to one of the polarizers. On the other hand, an ordered phase is dark when the director is parallel to either of the polarizers. Disordered (isotropic) phases are always dark irrespective of the orientation of the polarizers because the scattering by these phases does not change the polarization of the light. First, a two-dimensional directed columnar phase of 1.5 mM dispersion was observed with the polarized light microscopy. The dashed arrows indicate the orientation of the polarizers (Figure 6a and b). Figure 6a shows that the two-dimensional columnar phase blocked allof the light when one of the polarizers was parallel to the orientation of the columnar phase. We note that we deliberately rotated one of the polarizers a few degrees off from a perfect 90° in order to distinguish the well-oriented columns of stacks from the background. As a result, the background is not completely black. On the other hand, when both the analyzer and polarizer were rotated into a 45° orientation, light passed through the phase as seen in Figure 6b. We note that individual platelets lying parallel to the plane appeared as dark spots in Figure 6b.

In conclusion, we improved an existing synthesis method for synthesizing single-crystalline Au nanoplatelets into a high yield method with respect to platelets formed by using Ag nanoprisms as seeds. We assembled the 2D nano sheets into reversible flexible stacks by exploiting the secondary minimum

DOI: 10.1021/acs.nanolett.5b02384
Nano Lett. 2015, 15, 5617−5623

in the interaction potential between two parallel plates at a specific range (0.5−2.0 mM) of salt concentrations. Moreover, we demonstrated that the interplatelet distance in a column as well as the length of the columns can be controlled by varying the salt concentration from tens to hundreds of nanometers. With cryo-FIB-SEM, we were able to measure interplate distances in a particle stack. These experimental values were in a good agreement with our DLVO potential calculations. Next, we investigated the electric field directed self-assembly of the gold platelets in the absence and presence of salt. In absence of salt or at low salt concentrations, particles did not form stacks; they were aligned with their major axis in the field direction in a head-to-toe like fashion. On the other hand, at salt concentrations where the particles arranged into stacks, an electric field was seen to align them in the same direction, thus aligning the stacks perpendicularly to the external field. Moreover, the stacks further assembled into a columnar phase. As far as we know, such a control has not been demonstrated previously. The 2D regular patterns were seen to strongly polarize light, and further work is aimed at further exploring the tenability and optical properties of these intriguing self-assembled structures. Our system enables us to vary the interplate distance within a column by tuning the salt concentration such that a plasmon coupling can be realized.

MATERIALS AND METHODS

Synthesis and Characterization. We synthesized gold platelets by a modification of a procedure of Hachisu et al.[36] An important disadvantage of the original method of Hachisu et al.[36] was that the dispersions suffered from a low yield (less than 10% of particles, by number, are platelets in a typical synthesis), and a high degree of polydispersity both in size and shape as shown in Figure S6. We used silver platelets (Figure S1) as seeds to overcome this limitation. Ag nanoplatelets were synthesized in two steps by a method of Liz-Marzán et al.[47] We first synthesized small Ag nano particles as follows. In a closed 200 mL glass vial, 1 mL of 0.3 mM trisodium citrate (Sigma) was added to 100 mL of 0.1 mM silver nitrate (99%, Aldrich) solution. Next, 1 mL of 0.5 mM sodium borohydrate (Aldrich Sigma) was added under gentle stirring, and immediately followed by the addition 1 mL of a 5 wt % polyvinylpyrrolidone (Fluka, 15K) solution. Stirring was stopped when the solution turned to yellow. We used these Ag nano particles as seeds to synthesize silver nano platelets in a photochromic growth step. This step consisted of placing the suspension of silver seeds in 40 mL glass vials at a distance of about 3−4 cm from the light source (Philips Master TL Mini Super 80 8W/840) in a homemade photo reactor which consisted of 16 tube lights arranged in a rectangular box. These lights had emission bands at red (630 nm) and green (580 nm). The temperature inside the reactor was maintained at 40 °C. After 24 h, silver plates resulted as shown in Figure S1a. These particles were subsequently used as seeds for the gold platelets synthesis. Platelets with a width of submicron and a thickness of 16 nm were prepared as follows. In a dark room, 500 μL of Ag nanoplatelets solution was added to 25 mL of deionized water (18.2 MΩ cm, Millipore). Next, the suspension was mixed by shaking the vial for about 3−4 s followed by the addition of 5 mL of 10 mM aqueous chloroauric acid and 1.5 mL of filtered saturated salicylic acid solution. The solution was maintained in a thermostat water bath at 60 °C for 18 h. After the synthesis, the particle suspension was washed a couple of times with deionized water to remove smaller particles, and also unreacted species. In a typical synthesis 65% of hexagonal (and cut triangular), and 35% of triangular shaped particles were produced. Hexagonal and triangular shaped particles thus synthesized are shown in Figure 1a. The average edge length of the obtained triangular particles was 670 ± 65 nm, and hexagonal particles was 525 ± 45 nm. The thickness of the both particles was about 16 nm. We measured the surface potential of particles in water, and in a 30 wt % glycerol solution using a Malvern Zetasizer Nano. The surface potential of the particles was −35 mV in water and −40 mV in 30 wt % glycerol solution. Samples of gold particles of 1% by volume dispersed in deionized water were confined to glass capillaries with inner dimensions (cross section) of 0.1 mm × 1.0 mm or 0.1 mm × 2.0 mm (Vitrocom). The capillaries were cut to the desired length for each experiment. After filling the cell with the colloidal suspension, we sealed it with UV-curing optical adhesive (Norland no.68), and we studied particle dynamics by means of optical microscopy.

Electric-Field Setup. The electric cell consisted of a 0.1 mm × 1.0 mm or 0.1 mm × 2.0 mm cross section capillary with two 50 μm thickness nickel-alloy wires (Goodfellow) threaded along the side walls. We used a function generator (Agilent, model 3312 OA) and a wide band voltage amplifier (Krohn-Hite, model 7602M) to generate the electric fields. The field strength and the frequency were measured with an oscilloscope (Tektronix, model TDS3052).

(Cryo-) Focused Ion Beam-Scanning Electron Microscopy. Prior to the measurement, we mixed the gold suspension with 30 wt % of glycerol. Glycerol was used to prevent crystallization of water affecting colloidal structures. A droplet of the suspension was placed on a copper grid (typically used for transmission electron microscopy) and plunge-frozen in liquid nitrogen. Subsequently, the frozen samples were transferred under vacuum conditions to the FIB-SEM chamber, which was maintained at cryo-temperatures. The FIB-SEM (Nova Nanolab 600, FEI) was equipped with a cryo stage (PP2000, Quorum Technologies, Laughton). FIB milling conditions were 30 kV and 0.3 nA.

We used a scanning transmission electron microscopy (STEM), a FEI Tecnai 20F with a field emission gun (FEG), operating at 200 kV in high-angle annular dark-field mode (HAADF-STEM).

ASSOCIATED CONTENT

Supporting Information

The Supporting Information is available free of charge on the ACS Publications website at DOI: 10.1021/acs.nanolett.5b02384.

Additional SEM images of the particle synthesis, the details for the DLVO calculations, and electrodynamic instability of stacks (PDF)

Flexible 1D stacks of gold nanoplatelets at 0.8 mM of KCl (AVI)

Stacks directed to ordered structures using low field strength (AVI)

AUTHOR INFORMATION

Corresponding Authors

*(H.R.V) E-mail: H.R.Vutukuri@uu.nl.

*(A.v.B) E-mail: A.vanBlaaderen@uu.nl.

Notes

The authors declare no competing financial interest.

DOI: 10.1021/acs.nanolett.5b02384
Nano Lett. 2015, 15, 5617−5623

■ ACKNOWLEDGMENTS

We acknowledge B. W. Kwaadgras for useful assistance in DLVO potential calculations. We thank Da Wang for the STEM measurements and J. D. Meeldijk for the EDX measurements. H.R.V., and S. B., were part of the research program of the "Stichting voor Fundamenteel Onderzoek der Materie (FOM)", which is financially supported by the "Nederlandse organisatie voor Wetenschappelijke Onderzoek (NWO)". Part of this research was supported by the European Research Council under the European Union's Seventh Framework Programme (FP/2007-2013)/ ERC Grant Agreement no. (291667).

■ REFERENCES

(1) Burda, C.; Chen, X.; Narayanan, R.; El-Sayed, M. A. *Chem. Rev.* **2005**, *105*, 1025−1102.
(2) Xia, Y. N.; Xiong, Y. J.; Lim, B.; Skrabalak, S. E. *Angew. Chem., Int. Ed.* **2009**, *48*, 60−103.
(3) Sun, Y. G.; Xia, Y. N. *Science* **2002**, *298*, 2176−2179.
(4) Jain, P. K.; Huang, X. H.; El-Sayed, I. H.; El-Sayed, M. A. *Acc. Chem. Res.* **2008**, *41*, 1578−1586.
(5) Atwater, H. A.; Polman, A. *Nat. Mater.* **2010**, *9*, 205−213.
(6) Grzelczak, M.; Vermant, J.; Furst, E. M.; Liz-Marzan, L. M. *ACS Nano* **2010**, *4*, 3591−3605.
(7) Dreaden, E. C.; Alkilany, A. M.; Huang, X.; Murphy, C. J.; El-Sayed, M. A. *Chem. Soc. Rev.* **2012**, *41*, 2740−79.
(8) Grzelczak, M.; Perez-Juste, J.; Mulvaney, P.; Liz-Marzan, L. M. *Chem. Soc. Rev.* **2008**, *37*, 1783−91.
(9) Valentine, J.; Zhang, S.; Zentgraf, T.; Ulin-Avila, E.; Genov, D. A.; Bartal, G.; Zhang, X. *Nature* **2008**, *455*, 376−379.
(10) Shalaev, V. M. *Nat. Photonics* **2007**, *1*, 41−48.
(11) Ross, M. B.; Blaber, M. G.; Schatz, G. C. *Nat. Commun.* **2014**, *5*, 4090.
(12) Dong, A.; Chen, J.; Vora, P. M.; Kikkawa, J. M.; Murray, C. B. *Nature* **2010**, *466*, 474−477.
(13) Evers, W. H.; De Nijs, B.; Filion, L.; Castillo, S.; Dijkstra, M.; Vanmaekelbergh, D. *Nano Lett.* **2010**, *10*, 4235−4241.
(14) Henzie, J.; Grünwald, M.; Widmer-Cooper, A.; Geissler, P. L.; Yang, P. *Nat. Mater.* **2011**, *11*, 131−137.
(15) Young, K. L.; Jones, M. R.; Zhang, J.; Macfarlane, R. J.; Esquivel-Sirvent, R.; Nap, R. J.; Wu, J. S.; Schatz, G. C.; Lee, B.; Mirkin, C. A. *Proc. Natl. Acad. Sci. U. S. A.* **2012**, *109*, 2240−2245.
(16) Talapin, D. V.; Shevchenko, E. V.; Murray, C. B.; Kornowski, A.; Forster, S.; Weller, H. *J. Am. Chem. Soc.* **2004**, *126*, 12984−8.
(17) Abecassis, B.; Tessier, M. D.; Davidson, P.; Dubertret, B. *Nano Lett.* **2014**, *14*, 710−715.
(18) Mirkin, C. A.; Letsinger, R. L.; Mucic, R. C.; Storhoff, J. J. *Nature* **1996**, *382*, 607−609.
(19) Jones, M. R.; Macfarlane, R. J.; Lee, B.; Zhang, J. A.; Young, K. L.; Senesi, A. J.; Mirkin, C. A. *Nat. Mater.* **2010**, *9*, 913−917.
(20) Lalander, C. H.; Zheng, Y.; Dhuey, S.; Cabrini, S.; Bach, U. *ACS Nano* **2010**, *4*, 6153−6161.
(21) Jones, M. R.; Mirkin, C. A. *Angew. Chem., Int. Ed.* **2013**, *52*, 2886−91.
(22) Jones, M. R.; Seeman, N. C.; Mirkin, C. A. *Science* **2015**, *347*, 1260901−11.
(23) Gupta, S.; Zhang, Q.; Emrick, T.; Russell, T. P. *Nano Lett.* **2006**, *6* (9), 2066−9.
(24) Ryan, K. M.; Mastroianni, A.; Stancil, K. A.; Liu, H.; Alivisatos, A. P. *Nano Lett.* **2006**, *6*, 1479−82.
(25) Chen, J.; Dong, A.; Cai, J.; Ye, X.; Kang, Y.; Kikkawa, J. M.; Murray, C. B. *Nano Lett.* **2010**, *10*, 5103−8.
(26) Pietra, F.; Rabouw, F. T.; van Rhee, P. G.; van Rijssel, J.; Petukhov, A. V.; Erne, B. H.; Christianen, P. C.; de Mello Donega, C.; Vanmaekelbergh, D. *ACS Nano* **2014**, *8*, 10486−95.
(27) Murphy, C. J.; Sau, T. K.; Gole, A. M.; Orendorff, C. J.; Gao, J.; Gou, L.; Hunyadi, S. E.; Li, T. *J. Phys. Chem. B* **2005**, *109*, 13857−70.
(28) Bae, Y.; Kim, N. H.; Kim, M.; Lee, K. Y.; Han, S. W. *J. Am. Chem. Soc.* **2008**, *130*, 5432−5435.
(29) Zhou, Y.; Zhou, X. Z.; Park, D. J.; Torabi, K.; Brown, K. A.; Jones, M. R.; Zhang, C.; Schatz, G. C.; Mirkin, C. A. *Nano Lett.* **2014**, *14*, 2157−2161.
(30) Maier, S. A.; Brongersma, M. L.; Kik, P. G.; Meltzer, S.; Requicha, A. A. G.; Atwater, H. A. *Adv. Mater.* **2001**, *13*, 1501−1505.
(31) Ozbay, E. *Science* **2006**, *311*, 189−193.
(32) Eustis, S.; El-Sayed, M. A. *Chem. Soc. Rev.* **2006**, *35*, 209−217.
(33) Kang, Y.; Ye, X.; Chen, J.; Cai, Y.; Diaz, R. E.; Adzic, R. R.; Stach, E. A.; Murray, C. B. *J. Am. Chem. Soc.* **2013**, *135*, 42−5.
(34) Kang, Y.; Ye, X.; Chen, J.; Qi, L.; Diaz, R. E.; Doan-Nguyen, V.; Xing, G.; Kagan, C. R.; Li, J.; Gorte, R. J.; Stach, E. A.; Murray, C. B. *J. Am. Chem. Soc.* **2013**, *135*, 1499−505.
(35) Astruc, D.; Lu, F.; Aranzaes, J. R. *Angew. Chem., Int. Ed.* **2005**, *44*, 7852−7872.
(36) Okamoto, S.; Hachisu, S. *J. Colloid Interface Sci.* **1973**, *43*, 30−35.
(37) Millstone, J. E.; Park, S.; Shuford, K. L.; Qin, L. D.; Schatz, G. C.; Mirkin, C. A. *J. Am. Chem. Soc.* **2005**, *127*, 5312−5313.
(38) Patel, D.; James, K. T.; O'Toole, M.; Zhang, G.; Keynton, R. S.; Gobin, A. M. *J. Colloid Interface Sci.* **2015**, *441*, 10−6.
(39) Li, C. C.; Cai, W. P.; Cao, B. Q.; Sun, F. Q.; Li, Y.; Kan, C. X.; Zhang, L. D. *Adv. Funct. Mater.* **2006**, *16*, 83−90.
(40) Jiu, J. T.; Suganuma, K.; Nogi, M. *J. Mater. Sci.* **2011**, *46*, 4964−4970.
(41) Sun, X.; Dong, S.; Wang, E. *Angew. Chem., Int. Ed.* **2004**, *43*, 6360−3.
(42) Pienpinijtham, P.; Han, X. X.; Suzuki, T.; Thammacharoen, C.; Ekgasit, S.; Ozaki, Y. *Phys. Chem. Chem. Phys.* **2012**, *14*, 9636−41.
(43) Shankar, S. S.; Rai, A.; Ankamwar, B.; Singh, A.; Ahmad, A.; Sastry, M. *Nat. Mater.* **2004**, *3*, 482−488.
(44) Zhou, J.; Saha, A.; Adamcik, J.; Hu, H.; Kong, Q.; Li, C.; Mezzenga, R. *Adv. Mater.* **2015**, *27*, 1945−1950.
(45) Li, C. X.; Bolisetty, S.; Mezzenga, R. *Adv. Mater.* **2013**, *25*, 3694−3700.
(46) Chen, L.; Ji, F.; Xu, Y.; He, L.; Mi, Y. F.; Bao, F.; Sun, B. Q.; Zhang, X. H.; Zhang, Q. *Nano Lett.* **2014**, *14*, 7201−7206.
(47) Bastys, V.; Pastoriza-Santos, I.; Rodriguez-Gonzalez, B.; Vaisnoras, R.; Liz-Marzan, L. M. *Adv. Funct. Mater.* **2006**, *16*, 766−773.
(48) Sun, Y. G.; Xia, Y. N. *J. Am. Chem. Soc.* **2004**, *126*, 3892−3901.
(49) O'Brien, M. N.; Jones, M. R.; Kohlstedt, K. L.; Schatz, G. C.; Mirkin, C. A. *Nano Lett.* **2015**, *15*, 1012−7.
(50) Vutukuri, H. R.; Smallenburg, F.; Badaire, S.; Imhof, A.; Dijkstra, M.; van Blaaderen, A. *Soft Matter* **2014**, *10*, 9110−9119.
(51) Vutukuri, H. R.; Demirors, A. F.; Peng, B.; van Oostrum, P. D.; Imhof, A.; van Blaaderen, A. *Angew. Chem., Int. Ed.* **2012**, *51*, 11249−53.
(52) Smallenburg, F.; Vutukuri, H. R.; Imhof, A.; van Blaaderen, A.; Dijkstra, M. *J. Phys.: Condens. Matter* **2012**, *24*, 464113−10.
(53) Hermanson, K. D.; Lumsdon, S. O.; Williams, J. P.; Kaler, E. W.; Velev, O. D. *Science* **2001**, *294*, 1082−1086.
(54) Gangwal, S.; Cayre, O. J.; Velev, O. D. *Langmuir* **2008**, *24*, 13312−20.
(55) Shah, A. A.; Schultz, B.; Zhang, W.; Glotzer, S. C.; Solomon, M. J. *Nat. Mater.* **2014**, *14*, 117−124.
(56) Song, P.; Wang, Y.; Wang, Y.; Hollingsworth, A. D.; Weck, M.; Pine, D. J.; Ward, M. D. *J. Am. Chem. Soc.* **2015**, *137*, 3069−75.
(57) Leunissen, M. E.; Vutukuri, H. R.; van Blaaderen, A. *Adv. Mater.* **2009**, *21*, 3116−3120.
(58) Vutukuri, H. R.; Stiefelhagen, J.; Vissers, T.; Imhof, A.; van Blaaderen, A. *Adv. Mater.* **2012**, *24*, 412−6.
(59) Yethiraj, A. *Soft Matter* **2007**, *3*, 1099−1115.
(60) Mantegazza, F.; Caggioni, M.; Jimenez, M. L.; Bellini, T. *Nat. Phys.* **2005**, *1*, 103−106.
(61) Isambert, H.; Ajdari, A.; Viovy, J. L.; Prost, J. *Phys. Rev. Lett.* **1997**, *78*, 971−974.
(62) Hu, Y.; Glass, J. L.; Griffith, A. E.; Fraden, S. *J. Chem. Phys.* **1994**, *100*, 4674−4682.

DOI: 10.1021/acs.nanolett.5b02384
Nano Lett. 2015, 15, 5617−5623